Available online at www.sciencedirect.com
SCIENCE DIRECT
Journal of Catalysis 229 (2005) 499–512
JOURNAL OF CATALYSIS
www.elsevier.com/locate/jcat

Low-temperature water–gas shift: impact of Pt promoter loading on the partial reduction of ceria and consequences for catalyst design

Gary Jacobs [a], Uschi M. Graham [a], Emilie Chenu [a], Patricia M. Patterson [a], Alan Dozier [b], Burtron H. Davis [a,*]

[a] *Center for Applied Energy Research, 2540 Research Park Drive, Lexington, KY 40511, USA*
[b] *University of Kentucky Electron Microscopy Center, Chemical and Materials Engineering Department, A004 ASTeCC Building 0286, Lexington, KY 40506, USA*

Received 10 September 2004; revised 17 November 2004; accepted 25 November 2004

Available online 28 December 2004

Abstract

Partial reduction of ceria generates catalytically active bridging OH groups on the surface of ceria. Pt facilitates this surface reduction process, and in this work, the impact of the Pt promoter loading on catalyst structural-property relationships was explored. XANES spectra were recorded under H_2 treatment for a series of Pt/ceria catalysts with increasing Pt loading at both the Pt and Ce L_{III} edges. Reduction of Pt oxide was hindered by metal–support interactions, such that higher Pt loadings facilitated reduction of Pt oxide to Pt^0. Two routes of bridging OH group formation are as follows: (1) once it is reduced, Pt^0 dissociates H_2, which spills over to the ceria surface to generate the bridging OH group active sites directly, accompanied by a change in the oxidation state of the Ce atoms involved with the sites from Ce^{4+} to Ce^{3+}; and (2) H_2 or CO removes ceria surface capping oxygen atoms to generate vacancies (and surface Ce^{3+}), followed by H_2O dissociation at the vacancies to generate the bridging OH groups. Either route highlights the direct link between the extent of ceria partial reduction and the active site density of the bridging OH group active sites. The relative Ce^{3+} and Ce^{4+} concentrations from XANES were quantified and at low temperature; the greatest degree of ceria reduction was obtained for the Pt/ceria catalysts with higher Pt loadings, correlating with a higher bridging OH group active site density. Using in situ DRIFTS, we used CO as a probe molecule, as it reacts with the bridging OH groups to generate surface formates, the proposed intermediates of the WGS reaction. While addition of CO to the unpromoted catalyst reduced at 250 °C led to only very weak formate bands due to a lack of bridging OH groups on the ceria surface at that temperature, strong formate bands arose on the surface of the Pt/ceria catalysts at 250 °C. In situ DRIFTS was also utilized to probe the dynamics of the surface formate coverages under low-temperature WGS reaction conditions over the Pt/ceria series. A high H_2O/CO feed ratio was employed, and the surface formate coverages were found to be more limited by the WGS rate for the heavily loaded Pt/ceria catalysts. This indicates that Pt may not only serve to facilitate the generation of the bridging OH group active sites at low temperature, but may also be involved in accelerating surface formate decomposition, the elementary step of the mechanism that is proposed to be rate limiting. A clear trend of higher CO conversion with higher Pt loading was established in reaction testing. HR-TEM carried out on the 5%Pt/ceria catalyst indicated well-dispersed Pt clusters in the diameter range of 1–2 nm.

Keywords: Cerium oxide; CeO_2; Platinum; Water–gas shift; WGS; Low temperature; XANES; TEM

1. Introduction

Advanced low-temperature water–gas shift (WGS) catalysts are essential for the efficient generation of H_2, as steam reforming of hydrocarbons (e.g., natural gas, petroleum, or renewable resources) and the gasification of coal or biomass generates CO as an unwanted by-product. The high levels

* Corresponding author.
E-mail address: davis@caer.uky.edu (B.H. Davis).

0021-9517/$ – see front matter
doi:10.1016/j.jcat.2004.11.031

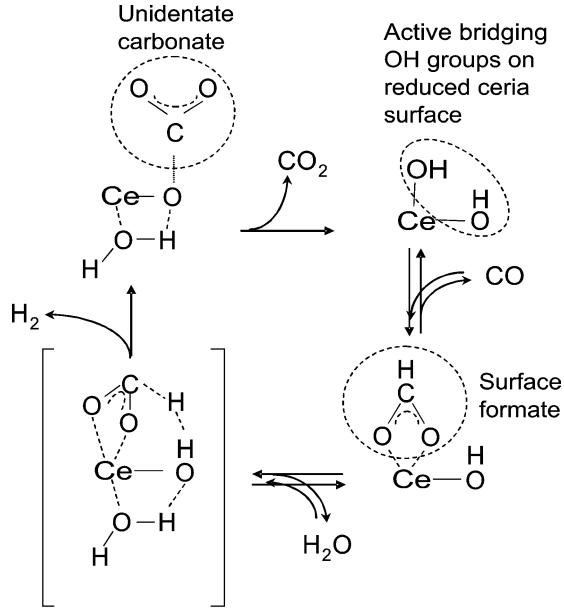

Scheme 1.

of CO produced by these processes demonstrate the need for WGS catalysts, as CO can be converted to CO_2 by reaction with H_2O, with the added benefit of generating more H_2. Another application for WGS catalysts is the conversion of CO to purify a hydrogen feed for a PEM fuel cell, as CO is a poison for the noble metal catalysts used in the electrodes [1–3]. WGS is an attractive option for CO conversion, but because it is exothermic, thermodynamics limits the equilibrium conversion at high temperatures. In contrast, at low temperatures, the thermodynamics are favorable but the reaction rate is constrained by kinetics, such that highly active catalysts are necessary to provide adequate activity. Typical designs of shift reactors are in stages, where high temperature shift (HTS) at 350–450 °C is conducted first to reduce, for example, 8–10% CO levels in the products from a methane steam reformer to about 3–5% CO, followed by a low-temperature WGS (LTS) at 150–250 °C, which can decrease the CO level to less than 1% [4]. Trace levels may be handled by a preferential oxidation (PROX) cleanup system. Currently, state-of-the-art WGS catalysts (e.g., commercial Cu/ZnO) do not meet the needs of the fuel cell industry. Therefore, the WGS reactor is still the heaviest and, spatially, the largest section of a fuel processor.

A key to the development of advanced catalysts lies in understanding the reaction mechanism and the nature of the active site. Recently we have conducted numerous studies with Pt/CeO_2 catalysts, and our findings support a low-temperature WGS reaction mechanism involving surface formate intermediates, as proposed by Shido and Iwasawa [5,6]. Their version of the reaction mechanism is shown in Scheme 1. The catalytically active sites were found to be Type II bridging OH groups [5–9] on partially reduced ceria, and these react with CO to generate surface formates. The relative stability of the formates at low temperature is

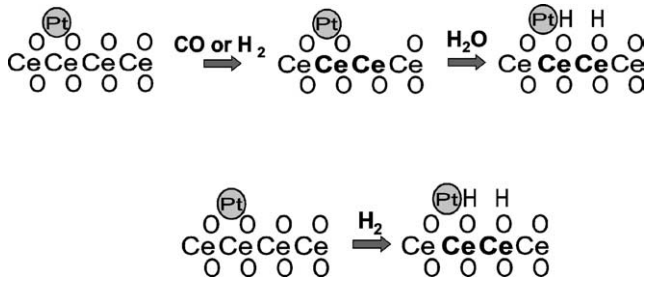

Scheme 2. Normal type Ce atoms, Ce^{4+}; bold **Ce** atoms, Ce^{3+}.

such that their decomposition is proposed to be the elementary step that is rate limiting. However, another important consideration is that mounting evidence suggests that H_2O promotes the forward decomposition rate of surface formates during WGS to H_2 and unidentate carbonate [5,6], which decomposes to CO_2 to regenerate the OH groups, completing the catalytic cycle. We have recently verified the autocatalytic role of H_2O in transient formate decomposition experiments [10]. A role of the metal (e.g., Pt, Rh) is to promote the surface reduction of ceria to generate the active bridging OH groups at lower temperatures [5,11]. Other possible roles of the noble metal remain to be defined.

In Scheme 2, the top figure shows that removal of surface capping oxygen atoms in the ceria surface shell will cause a lowering of the oxidation state of Ce atoms involved with the vacancy from Ce^{4+} to Ce^{3+}. Under conditions that are net reducing, dissociative adsorption of water at the vacancy generates the bridging OH groups, maintaining the Ce^{3+} oxidation state on the ceria atoms associated with the oxygen deficiency. Recently we have observed the formation of the bridging OH groups after reduction pretreatment with CO, followed by treatment with H_2O. However, we also assume that once Pt is in the metallic state, Pt^0 is able to dissociate H_2 at relatively low temperatures, with hydrogen spilling over to the ceria surface to form OH groups, a process that is accompanied by a change in oxidation state of Ce atoms involved with the bridging OH groups from Ce^{4+} to Ce^{3+}. This is indicated by the bottom schematic of Scheme 2. This possibility [10] is suggested by the fact that D_2 rapidly dissociates, spills over, and exchanges with H over the surface of partially reduced ceria (promoted with Pt) at low temperatures to replace the bridging OH groups with OD.

In this work, the influence of Pt loading on the degree of ceria partial reduction in the low-temperature range was investigated by in situ XANES at the Ce L_{III} edge. As metal–support interactions often hinder the reduction of promoters, rendering them less effective, the reduction of Pt oxide was also examined by in situ XANES, at the L_{III} edge of Pt.

In this work, the presence of Type II bridging OH groups was investigated by in situ DRIFTS spectroscopy over the series of Pt/ceria catalysts in the low-temperature range. Furthermore, CO was used as a probe molecule for the presence of bridging OH groups, as it reacts with them to generate surface formate. This technique is useful because, in the absence of the second reactant, water, the surface for-

mates are quite stable at low temperatures. To determine whether Pt plays a direct role in the catalytic mechanism, in situ DRIFTS was also utilized to probe the dynamics of the formate coverages over the Pt/ceria series. Finally, size and morphology aspects of both the platinum and ceria components were characterized by high-resolution transmission electron microscopy (HR-TEM).

2. Experimental

2.1. Catalyst preparation

High-surface-area ceria was prepared via homogeneous precipitation from the nitrate in urea with aqueous ammonia in a procedure similar to that of Li et al. [12], whereby urea decomposition is a slow process resulting in a more homogeneous precipitation. Appropriate amounts of $Ce(NO_3)_3 \cdot 6H_2O$ (Alfa Aesar, 99.5%) and urea (Alfa Aesar, 99.5%) were dissolved in 900 cm^3 of deionized water, and to this solution about 30 cm^3 NH_4OH (Alfa Aesar, 28–30% NH_3) was added dropwise (∼1 cm^3/min). The mixture was then heated at 100 °C with constant stirring. The precipitate was filtered, washed with 600 cm^3 of boiling deionized water, and dried in an oven at 110 °C overnight. The dried precipitate was then crushed and calcined in a muffle furnace at 400 °C for 4 h. Pt was added by incipient wetness impregnation of tetraammine platinum (II) nitrate (Alfa Aesar). The resulting catalyst was dried at 110 °C for 24 h and then calcined at 400 °C for 4 h.

2.2. BET surface area

BET surface area measurements were made with a Micromeritics Tristar 3000 gas adsorption analyzer. In each trial, a weight of approximately 0.25 g of sample was used. Nitrogen adsorption was carried out at its boiling temperature.

2.3. Temperature-programmed reduction and thermogravimetric analysis

Temperature-programmed reduction (TPR) was conducted on unpromoted and platinum-promoted ceria catalysts in a Zeton–Altamira AMI-200 unit, which was equipped with a thermal conductivity detector (TCD). Argon was used as the reference gas, and 10% H_2 (balance Ar) was flowed at 30 cm^3/min as the temperature was increased from 50 to 800 °C at a ramp rate of 10 °C/min.

Temperature-programmed treatment was also undertaken with a Seiko Instruments Inc. TG/DTA 320 Simultaneous thermogravimetric/differential thermal analyzer coupled to a Micromass PC residual gas analyzer. A known quantity of catalyst (ca. 100 mg) was placed in a Pt sample pan and heated at 10 °C/min to 750 °C in a reducing flow of 20% v/v H_2/He, after it had been kept at 100 °C for 30 min to dry the sample, while the effluent gas was monitored over the mass range 10–100.

2.4. X-ray absorption near-edge spectroscopy

X-ray absorption near-edge spectroscopy (XANES) spectra at the Pt L_{III} (11564 eV) and Ce L_{III} (5723 eV) edges were recorded at Beamline X-18b at the National Synchrotron Light Source (NSLS) at Brookhaven National Laboratory (BNL) in Upton, New York. A crystal detuning procedure was used to prevent glitches arising from harmonics. The second crystal of the channel cut monochromator is weakly linked to the crystal and slightly spring-loaded. The other side is a picomotor, a very fine high-pitch screw that turns by piezo, which allows for slight detuning of the crystal. The X-ray ring at the NSLS can produce a flux of 1×10^{10} photons/s at 100 mA and 2.8 GeV, and its energy range capability at X18b is 5.5–40 keV. We determined the sample thickness by calculating the amount of sample, ω_D, in grams per square centimeter, with the thickness equation,

$$\omega_D = \ln(I_o/I_t) \Big/ \sum (\mu/\rho)_j w_j,$$

where μ/ρ is the total cross section (absorption coefficient/density) of element j in the sample at the absorption edge of the EXAFS element under study in cm^2/g, w_j is the weight fraction of element j in the sample, and $\ln(I_o/I_t)$ was taken over a typical range of 1 to 2.5. An average value of ω_D obtained from the input of both values was used. Based on the calculation for ω_D, and the cross-sectional area of the pellet, we calculated the mass in grams. Boron nitride was utilized in many cases to dilute the sample, such that the wafer could be self-supported. A typical catalyst mixture with boron nitride at a ratio of 1:10 with a total sample mass of approximately 0.27 g was not uncommon. Smooth self-supporting pellets, free of pinholes, were pressed and loaded into the in situ XAS flow cell, and the treatment gas was directed right to the sample area. After the cell was purged for a long time with inert gas at a high flow rate to ensure removal of air, the samples were treated in situ at the beamline with a hydrogen/helium mixture (150 cm^3/min H_2 and 500 cm^3/min He) during heating at 10 °C/min in the temperature range 20 to 300 °C. Scans were obtained in transmission mode at 50 °C intervals to explore the partial reduction of ceria and the reduction of the platinum promoter. The UHP H_2 and He gases were mixed in a manifold and passed through an oxygen/water trap before feeding to the cell. Raw data were processed to give the normalized XANES spectra. Linear-combination XANES fits of treated catalysts with reference standards were carried out with the WinXAS program [13].

2.5. High-resolution transmission electron microscopy

High-resolution transmission electron microscopy (HRTEM) measurements were carried out with a JEOL

2010F FasTEM field emission electron microscope equipped with an energy-dispersive X-ray (EDX) detector and operated at an accelerating voltage of 200 kV. The electron beam has a point-to-point resolution of 0.5 nm. Before HRTEM analysis the Pt-promoted and unpromoted ceria samples were reduced ex situ in flowing hydrogen at 300 °C for 10 h and subsequently passivated at room temperature. Catalyst powder was lightly dusted onto 200-mesh Cu grids coated with lacy carbon.

2.6. Diffuse reflectance infrared Fourier transform spectroscopy

A Nicolet Nexus 870 was used, which was equipped with a DTGS-TEC detector. A high-pressure/high-temperature chamber fitted with ZnSe windows was utilized as the WGS reactor for in situ reaction measurements. The gas lines leading to and from the reactor were heat traced, insulated with ceramic fiber tape, and further covered with general-purpose insulating wrap. Scans were taken at a resolution of 4 to give a data spacing of 1.928 cm^{-1}. Typically, 128 scans were taken to improve the signal-to-noise ratio. The sample amount utilized was 33 mg.

A steam generator consisted of a downflow tube packed with quartz beads and quartz wool heated by a ceramic oven and equipped with an internal thermocouple. The lines after the steam addition were heat traced. The steam generator and lines were run at the same temperature as that of the in situ sample holder of the DRIFTS cell. Water was pumped with a precision ISCO model 500D syringe pump into a steam generator via a thin needle welded to a 1.6-mm line.

Feed gases (UHP) were controlled with Brooks 5850 series E mass flow controllers. Iron carbonyl traps consisting of lead oxide on alumina (Calsicat) were placed on the CO gas line. All gas lines were filtered with Supelco O_2/moisture traps. During CO adsorption, the flows were maintained at 3.75 cm^3/min CO and 135 cm^3/min N_2. During WGS testing, 125 cm^3/min of the nitrogen balancing gas was replaced by steam.

2.7. Testing in a fixed-bed reactor

Steady-state CO conversion measurements were conducted in a fixed-bed reactor consisting of a 0.5-in. stainless-steel tube with an internal thermocouple. Experiments were conducted with 33 mg of catalyst diluted to 0.4 g with silica. The catalyst bed was supported on a bed of quartz glass wool. A description of the steam generator, gas delivery system, and ancillary equipment is provided in Section 2.6. The conditions were chosen to mimic those of the low-temperature shift reactor of a fuel processor, with the exception that CO_2 was not included in the tests. The gas flows were 3.75 cm^3/min CO, 125 cm^3/min H_2O, 100 cm^3/min H_2, and 10 cm^3/min of N_2. Catalysts were activated in H_2 (100 cm^3/min at 300 °C) before reaction testing.

Table 1
Bet surface area and porosity measurements from physisorption of nitrogen at 77 K

Sample name	BET SA (m^2/g)	Pore volume (cm^3/g)	Average pore radius (nm)
Unpromoted ceria	125	0.0909	1.45
0.5%Pt/ceria	117	0.0843	1.53
1.0%Pt/ceria	116	0.0871	1.50
2.5%Pt/ceria	114	0.0896	1.57
5.0%Pt/ceria	117	0.0894	1.53

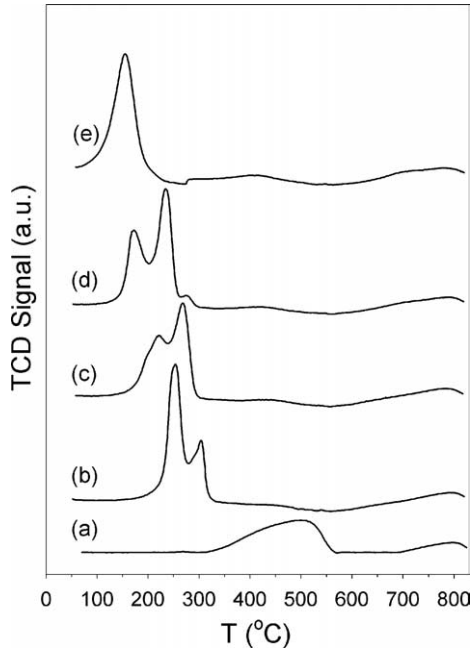

Fig. 1. TPR profiles (moving upward) of (a) unpromoted ceria; (b) 0.5%Pt/ceria; (c) 1.0%Pt/ceria; (d) 2.5%Pt/ceria; and (e) 5.0%Pt/ceria.

3. Results

3.1. Standard characterization

Table 1 provides the results of nitrogen physisorption. The BET surface area of the starting unpromoted ceria material was 125 m^2/g. After platinum loading and following the second calcination step, the surface areas of all of the catalysts were between 114 and 117 m^2/g. There was a slight increase in the average pore radius from 1.45 nm to between 1.50 and 1.60 nm, which is typical following the loading of a metal to an oxide and is likely due to blocking of the narrowest pores by the metal.

TPR profiles of the unpromoted and Pt-promoted ceria samples are displayed in Fig. 1. High-surface-area ceria materials usually have two distinct features in hydrogen TPR, a peak close to 750 °C that is assigned to the bulk reduction from CeO_2 to Ce_2O_3, and a broader peak situated close to 450 °C that is typically assigned to a surface reduction process. As has been noted in previous work [6,11,14,15], the addition of metals can catalyze the surface reduction process, shifting the broad peak to lower temperatures and

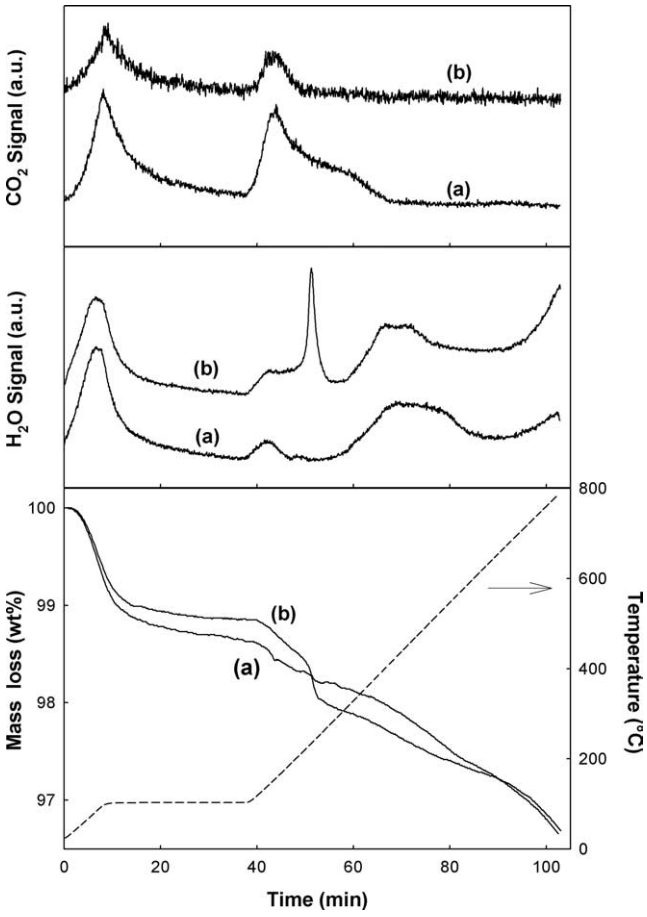

Fig. 2. Mass loss and mass spectrometer profiles for H_2O and CO_2 for (a) unpromoted ceria and (b) Pt/ceria catalysts.

sharpening its features, while not measurably affecting bulk ceria reduction. Yao and Yao [15] indicated that the surface reduction probably involves the removal of surface capping oxygen atoms from ceria. However, it has also been reported that bridging-type OH groups are formed after a hydrogen surface reduction process not only for metal/ceria catalysts, but for other partially reducible oxides as well, including zirconia-based [16] and thoria-based [8,17] catalysts. These groups can form either via a route whereby water can dissociate at a vacancy (e.g., after CO was used to reduce the ceria surface, water addition resulted in the formation of the bridging OH groups [18]), as shown in Scheme 2, or even directly via the spillover of dissociated hydrogen from Pt to the ceria surface, as depicted in Scheme 2. In either case, two ceria atoms must change oxidation state for every defect site (i.e., vacancy or corresponding bridging OH pair) formed. Noble metal addition has been found to facilitate bridging OH group formation [5,18].

TGA-MS results are displayed in Fig. 2. Thermal treatment in a flow of hydrogen produces a more rapid decrease in mass for the Pt/ceria catalyst than for the unpromoted catalyst, evolving H_2O ($m/e = 18$) and CO_2 ($m/e = 44$) during the reduction process. The signal obtained for CO_2 was approximately 2 orders of magnitude less than that for the H_2O. Negligible quantities of CO ($m/e = 28$) were observed. For Pt/ceria, CO_2 evolved until a temperature of 250 °C was attained, whereas CO_2 was found to evolve up to a much higher temperature of 450 °C for the unpromoted catalyst. For both unpromoted and Pt/ceria, H_2O evolution included a small peak at < 200 °C, attributed to desorption of physisorbed water. However, in the higher temperature region, whereas a very broad peak was observed for unpromoted ceria over the range of 300–600 °C, two narrower peaks were observed for Pt/ceria. A sharp low-temperature peak occurred between 250 and 300 °C, and a broader peak was observed over the range 300–500 °C. The mass loss experienced over the 250–300 °C region of the mass loss profile was slightly larger ($\sim 0.4\%$) than that expected if the loss were due solely to platinum reduction alone ($\sim 0.2\%$). The results agree very well qualitatively with the TPR data and suggest that partial reduction of ceria was promoted to lower temperature in the presence of the noble metal promoter. In this activation process, the data suggest that Pt facilitates the decomposition of surface carbonate species (i.e., decarboxylation) as CO_2.

3.2. X-ray absorption near-edge spectroscopy

To directly monitor the reduction of the catalyst in H_2, in situ XANES was employed, as the white line provides information about the density of unoccupied states above the Fermi level. L_{III} edges of both Pt and Ce were scanned; the transitions were from $2p_{3/2}$ core states to unoccupied $5d$ levels.

For the case of Pt ($L_{III} = 11{,}564$ eV), the PtO_2 and Pt^0 standards are displayed in Fig. 3A, and the intense white line of the oxide is readily apparent. Figs. 3B–D compare the changes in the Pt white line of the Pt/ceria catalysts as a function of Pt loading during reduction in H_2. The more heavily loaded catalysts offer a more facile reduction of Pt oxide. Whereas Pt reduction is virtually complete between 250 and 300 °C for the 0.5% Pt-loaded sample, Pt reduction is already complete at 250 °C for 2.5% Pt/ceria, and the Pt clusters on the 5% Pt/ceria catalyst are almost completely reduced by 100 °C. The results are consistent with a metal–support interaction between Pt and ceria, which hinders Pt oxide reduction at low loadings, where interactions between metal and oxide are greatest.

As discussed previously, the impact of Pt in promoting the reduction of the ceria surface shell to produce the active bridging OH groups is of even greater interest, as formation of the Type II bridging OH groups is a surface reduction process, accompanied by a change in the oxidation state of the Ce atoms involved with the bridging OH group sites from Ce^{4+} to Ce^{3+} (i.e., partial reduction of ceria). Therefore, the Ce L_{III} edge ($L_{III} = 5723$ eV) was also examined for each catalyst over a series of reduction temperatures in flowing hydrogen. As displayed in Fig. 4A, the XANES lineshapes of Ce^{3+} and Ce^{4+} oxidation states are very different. Peak C for Ce^{4+} has been assigned to absorption into the $5d$ level

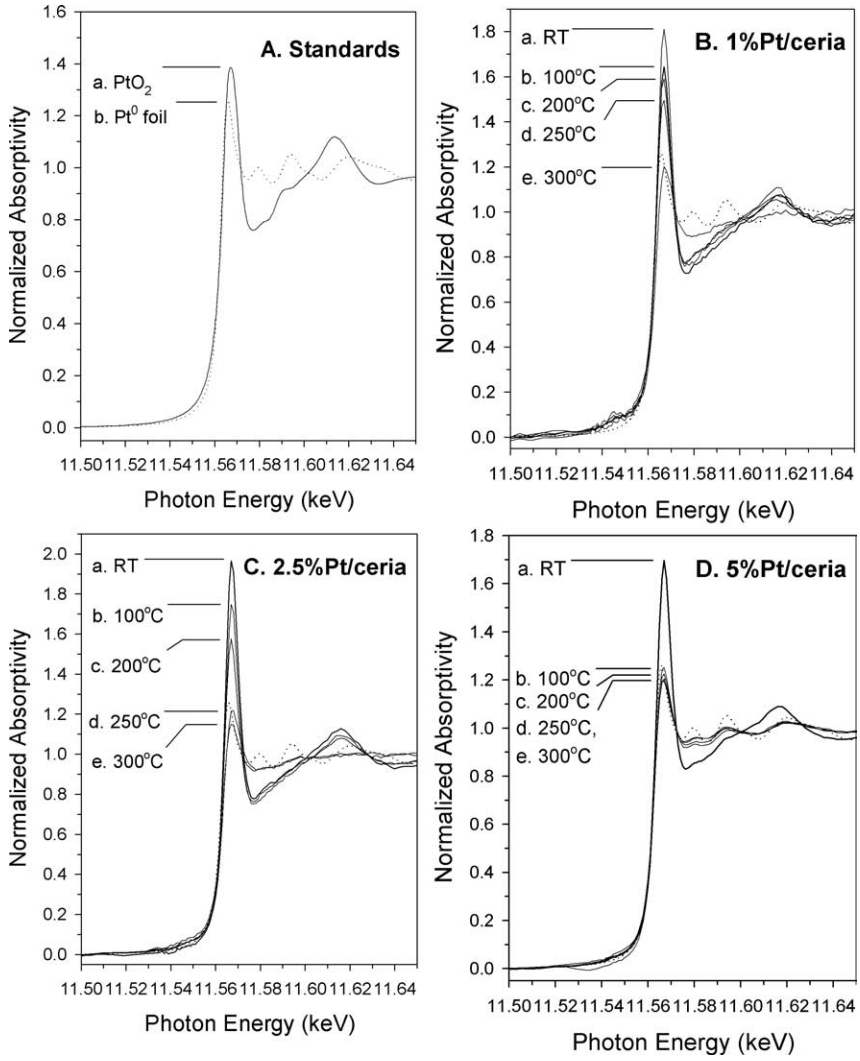

Fig. 3. XANES spectra at Pt L_{III} edge for (A) references and the reduction of Pt/ceria catalysts, including (B) 1%Pt/ceria, (C) 2.5%Pt/ceria, and (D) 5.0%Pt/ceria at temperatures ranging from (a) room temperature (RT) to (e) 300 °C.

with no occupancy in $4f$ for either the initial or final state, and, while present in completely oxidized CeO_2, it is virtually absent for Ce^{3+}. The final state configuration may be written Ce $[2p^5 4f^0 5d^1]$ O $[2p^6]$. The peak labeled B is split into at least two separate assignments [19,20]. Peak B_1, also present in the CeO_2 sample (i.e., Ce^{4+}), has been assigned to absorption into the $4f$ level in the final state. That is, in addition to an electron excited from the Ce $2p$ shell to the $5d$ shell, another electron is excited, coming from the valence band (i.e., the O $2p$ shell) to the Ce $4f$ shell, leaving a hole in the valence band. For the sake of brevity, the simplest final state configuration associated with B_1 may be written Ce $[2p^5 4f^1 5d^1]$ O $[2p^5]$. During reduction, peaks B_1 and C decrease and a new peak, B_0, develops, occurring just below that of B_1, and associated with absorption into the $5d$ level, with $4f$ occupancy in the initial state. Its final state configuration may be written Ce $[2p^5 4f^1 5d^1]$ O $[2p^6]$. The intensity of B_0 is very high for any Ce^{3+} reference, with one example (cerous carbonate) provided in Fig. 4A. These key features (B_0 for Ce^{3+} and both B_1 and C as a fingerprint for Ce^{4+}) were used to gain insight into the degree of reduction of the ceria catalyst component.

We quantified the degree of reduction of ceria by carrying out a linear combination fitting of XANES spectra for treated catalysts with WinXAS [13], with reference compounds for Ce^{3+} and Ce^{4+} oxidation states, in the range of 5.70 and 5.77 keV. Results of the fitting procedure are reported in Table 2. For unpromoted ceria, the ceria remains relatively unreduced in H_2 treatment at 300 °C (Fig. 4B), with only about 8% of cerium atoms in the Ce^{3+} oxidation state. However, with just 0.5% Pt, changes are evident that are consistent with partial reduction of ceria at temperatures between 250 and 300 °C (increasing the percentage of cerium atoms in the Ce^{3+} oxidation state from 7.5 to 24%). With increasing Pt promoter loading, the reduction of the surface shell is further facilitated (i.e., it shifts to a lower temperature). With 1% Pt and 2.5% Pt, the major change in the partial reduction of ceria occurs between 200 and 250 °C

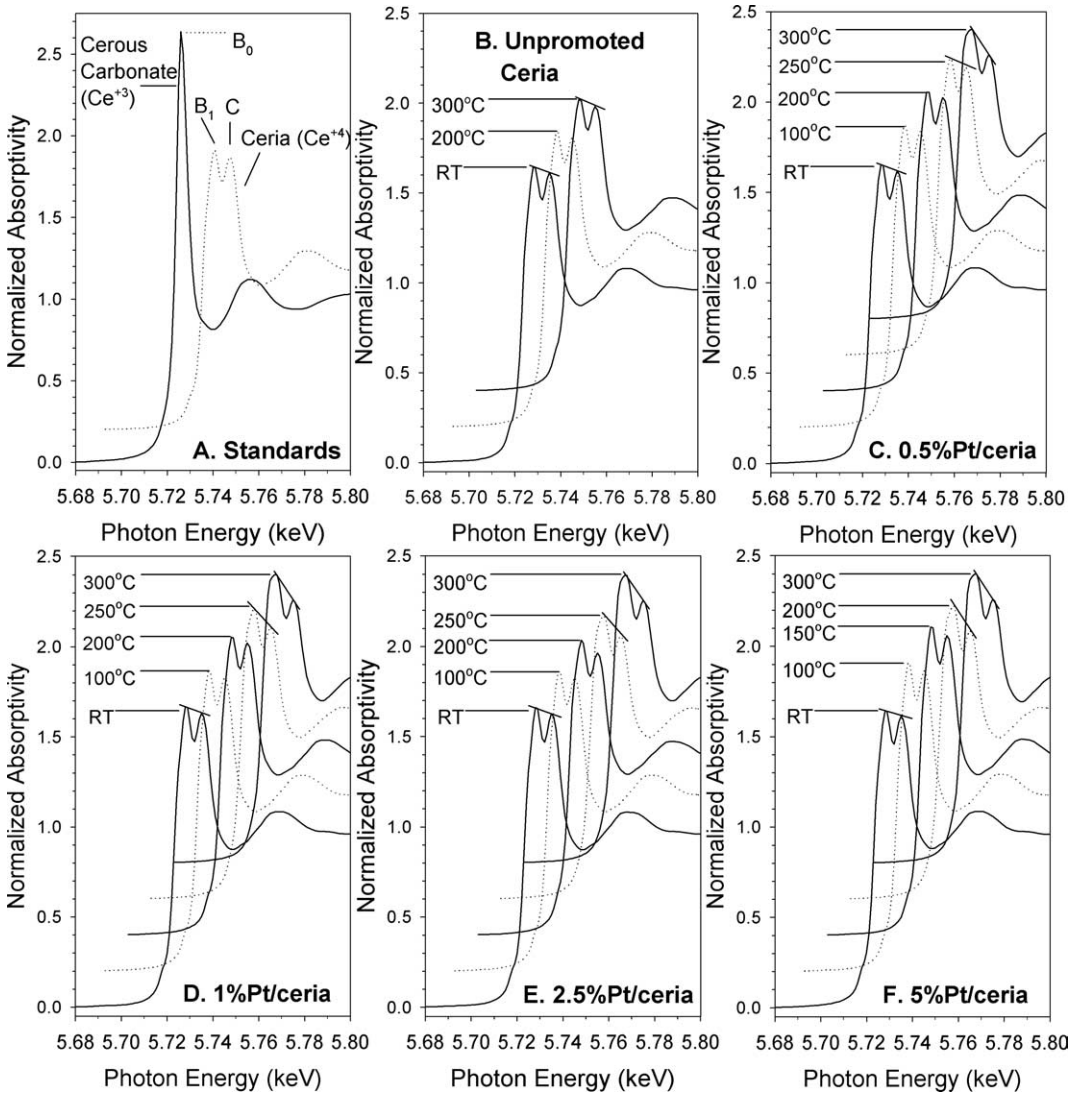

Fig. 4. XANES spectra at Ce L_{III} edge for (A) references and the reduction of Pt/ceria catalysts, including (B) unpromoted, (C) 0.5%Pt/ceria, (D) 1%Pt/ceria, (E) 2.5%Pt/ceria, and (F) 5.0%Pt/ceria. Note that the shifts in energy are not real. The spectra are staggered for ease of viewing the lineshape differences.

Table 2
Linear combination fits of XANES spectra with the Ce^{3+} and Ce^{4+} reference compounds

T (°C)	No Pt		0.5%Pt		1.0%Pt		2.5%Pt		5.0%Pt	
	Ce^{3+}	Ce^{4+}	Ce^{3+}	Ce^{4+}	Ce^{3+}	Ce^{4+}	Ce^{3+}	Ce^{4+}	Ce^{3+}	Ce^{4+}
RT	2.9	97.1	1.1	98.9	0.8	99.2	0.9	99.1	0.5	99.5
100	–	–	2.2	97.8	2.8	97.2	2.9	97.1	1.0	99.0
150	–	–	–	–	–	–	–	–	3.1	96.9
200	4.9	95.1	3.5	96.5	4.1	95.9	10.7	89.3	21.0	79.0
250	–	–	7.5	92.5	17.4	82.6	22.1	77.9	–	–
300	8.1	91.9	24.0	76.0	24.1	75.9	24.1	75.9	25.0	75.0

Relative percentages as a function of reduction temperature. Reduction carried out in hydrogen.

(4.1 to 17.4% and 10.7 to 22.1%, respectively), and with 5% Pt, the change for the most part occurs between 150 and 200 °C (3.1 to 21%). A sample linear combination fit is provided in Fig. 5 for the 2.5% Pt/ceria catalyst treated at 200 °C in hydrogen.

The results are consistent with the hypothesis that enhanced partial reduction of ceria is attributed to the promotion by Pt. As partial reduction of ceria is not facilitated until Pt^0 is formed, this finding suggests that the partial reduction of ceria is likely a direct result of spillover of dissociated H_2 from Pt^0 to the surface of ceria. This would allow the bridging OH groups to be formed directly, a process accompanied by the reduction of the cerium atoms in the surface shell from Ce^{4+} to Ce^{3+}, as shown in Scheme 2.

3.3. High-resolution transmission electron microscopy

With partially reducible oxides, in the presence of a metal promoter, it is difficult to obtain crystallite size and metal dispersion values with standard chemisorption methods. In this case, advanced electron microscopy can provide useful information on the metal promoter, the oxide nanostructure

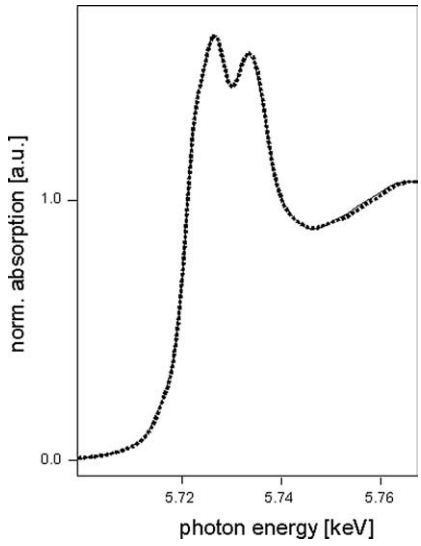

Fig. 5. Sample linear combination XANES fitting with Ce^{3+} and Ce^{4+} reference compounds for 2.5%Pt/ceria after reduction in hydrogen at 200 °C.

and surface, and the interface between the two domains. Figs. 6A and B present HRTEM images for the unpromoted and 5% Pt/CeO_2 samples, obtained in the plane view imaging mode. The two columns show agglomerates of ceria nanoparticles with increasing magnification from top to bottom (the arrows in the images illustrate the regions being magnified). The agglomerates are typically composed of 5–8 nm diameter ceria particles that exhibit a strong tendency to align and form elongated ridges and channels. The agglomerates were found to range in size from tens of nanometers to approximately half a micrometer. At the higher magnifications it is evident from the lattice fringes that the individual ceria nanoparticles are well crystallized. The majority of the dark spots visible in the HRTEM images are not Pt nanoparticles, as they are also present in the unpromoted samples, but are caused by grain boundary and density effects. It is possible for one to enhance the visibility of the Pt nanoparticles by tilting the sample away from the strong diffraction conditions of the crystalline ceria and employing a minimum-contrast technique. The Pt particles (indicated by the arrows) are clearly visible in Fig. 6C (corresponding to the 5% Pt loaded catalyst), and their presence was confirmed by EDX analysis. The EDX spectrum shown in Fig. 6C corresponds to the encircled Pt particle. The nanoparticles of Pt exhibit diameters in the 1–2 nm range and appear to be evenly and well dispersed over the ceria surface.

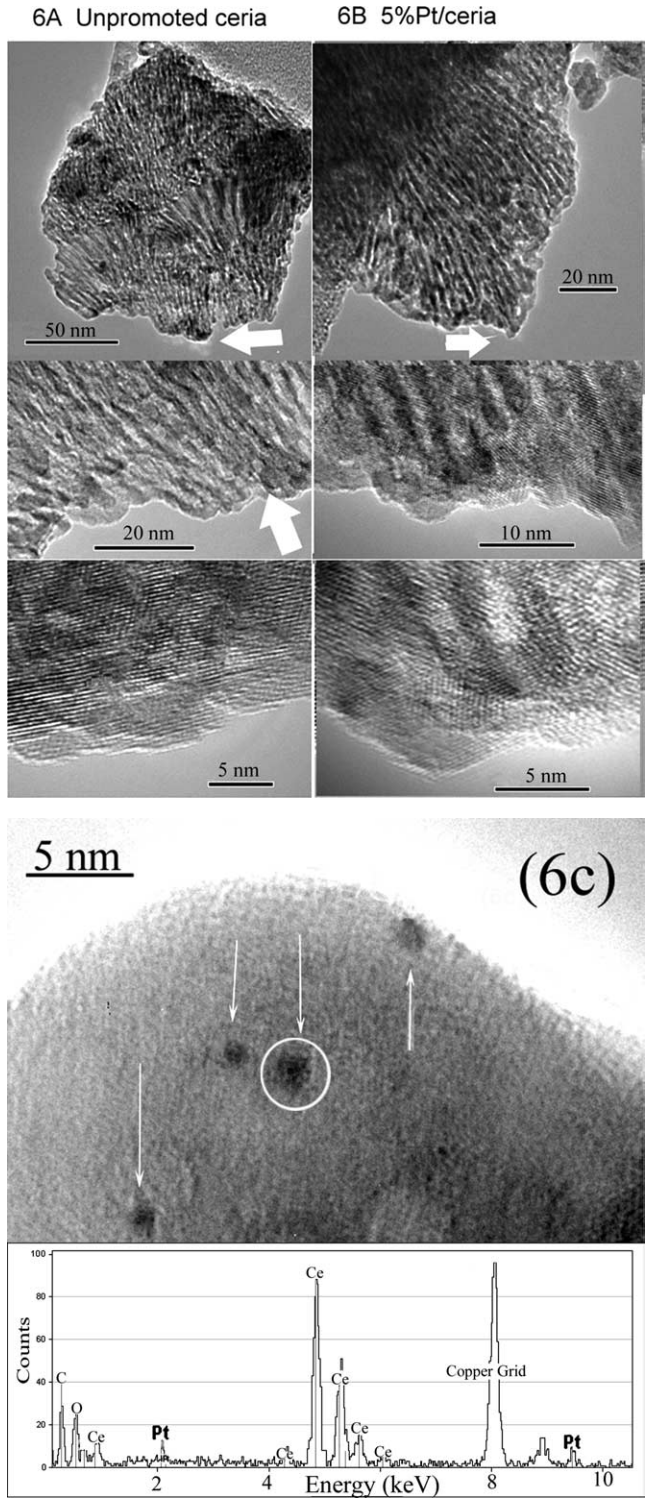

Fig. 6. (A) HRTEM images of unpromoted CeO_2, (B) HRTEM images of 5%Pt/CeO_2, (the arrows show the areas magnified). (C) HRTEM images of Pt clusters on the surface of ceria for the 5%Pt/ceria catalyst.

3.4. In situ diffuse reflectance infrared Fourier transform spectroscopy

The results from in situ infrared spectroscopy are first reported for the study of the impact of the Pt promoter loading. These include spectra for (1) the surface reduction process (Figs. 7A and B); (2) the adsorption of CO (Figs. 8A–D); and (3) the response of surface species to the WGS reaction (Figs. 8B and D). With increasing Pt loading, background absorption became a problem, and especially in the case of the 5% Pt/ceria sample. Therefore, the graphs for the 5% Pt/ceria sample are considered separately in Figs. 8D.

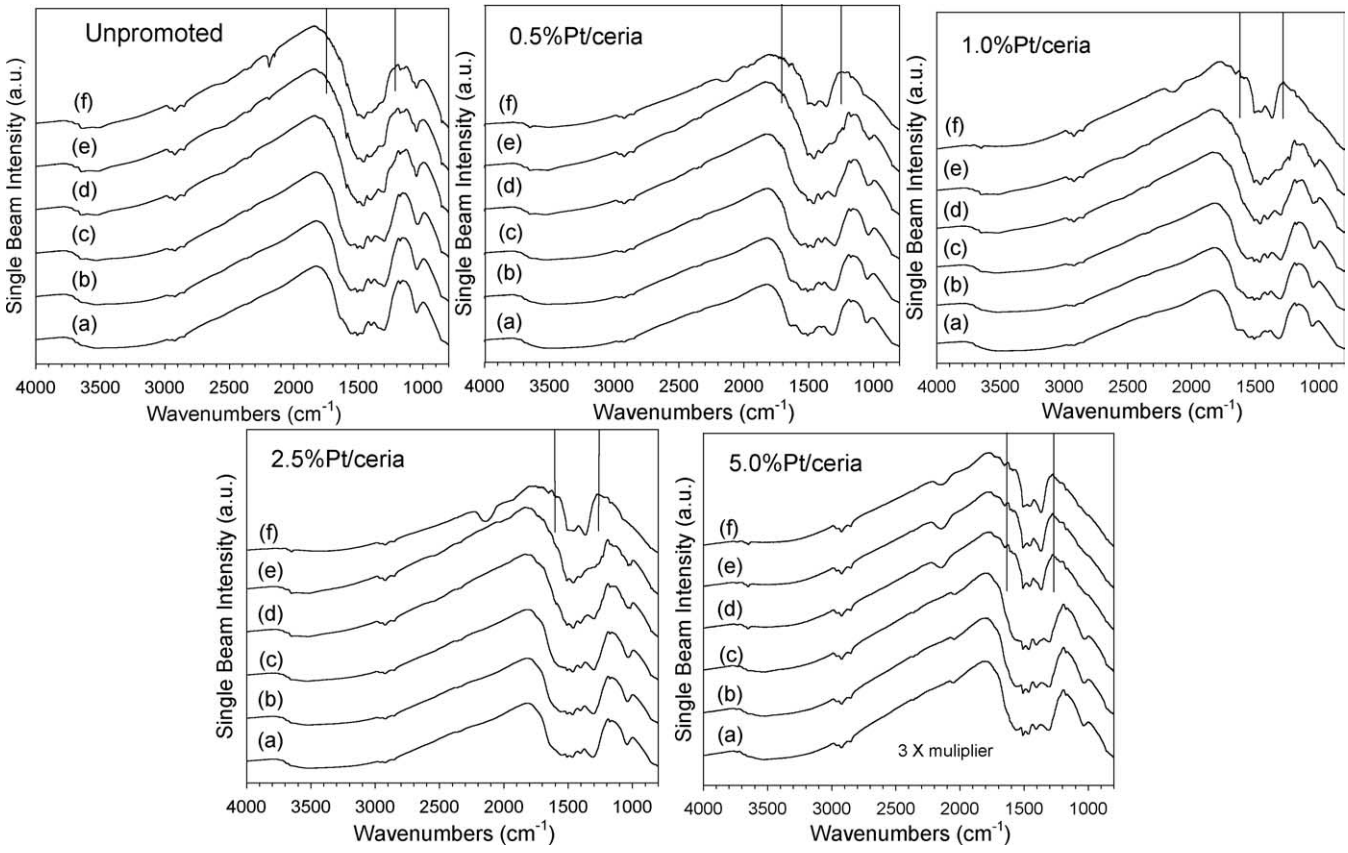

(A)

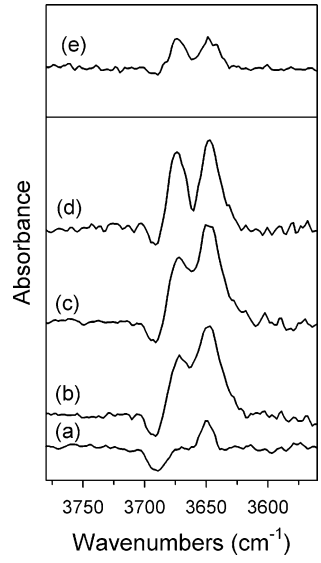

(B)

Fig. 7. (A) Single beam intensity DRIFTS spectra for the reduction in hydrogen of unpromoted and Pt/ceria catalysts of varying loading of Pt at (a) room temperature; (b) 75; (c) 100; (d) 150; (e) 200; and (f) 250 °C. (B) Absorbance spectra of the OH region for the reduction of unpromoted and Pt/ceria catalyst of varying loading in hydrogen, including (a) unpromoted; (b) 0.5%Pt/ceria; (c) 1.0%Pt/ceria; (d) 2.5%Pt/ceria; and (e) 5.0%Pt/ceria.

3.4.1. Ceria surface reduction process

As discussed previously, the surface reduction process involves at least three stages: (1) the reduction of the promoter; (2) the reduction of the ceria surface to yield bridging OH groups (3650 cm^{-1}); and (3) the removal of surface carbonate species. Carbonate removal is suggested by the disappearance of bands at ca. 1050 cm^{-1} (carbon–oxygen), 1400 cm^{-1} (OCO), and 1600 cm^{-1} (OCO) and the appearance of bands at ca. 2000 cm^{-1} and 2150 cm^{-1}, which are consistent with Pt–CO and Ce–CO. The width of ab-

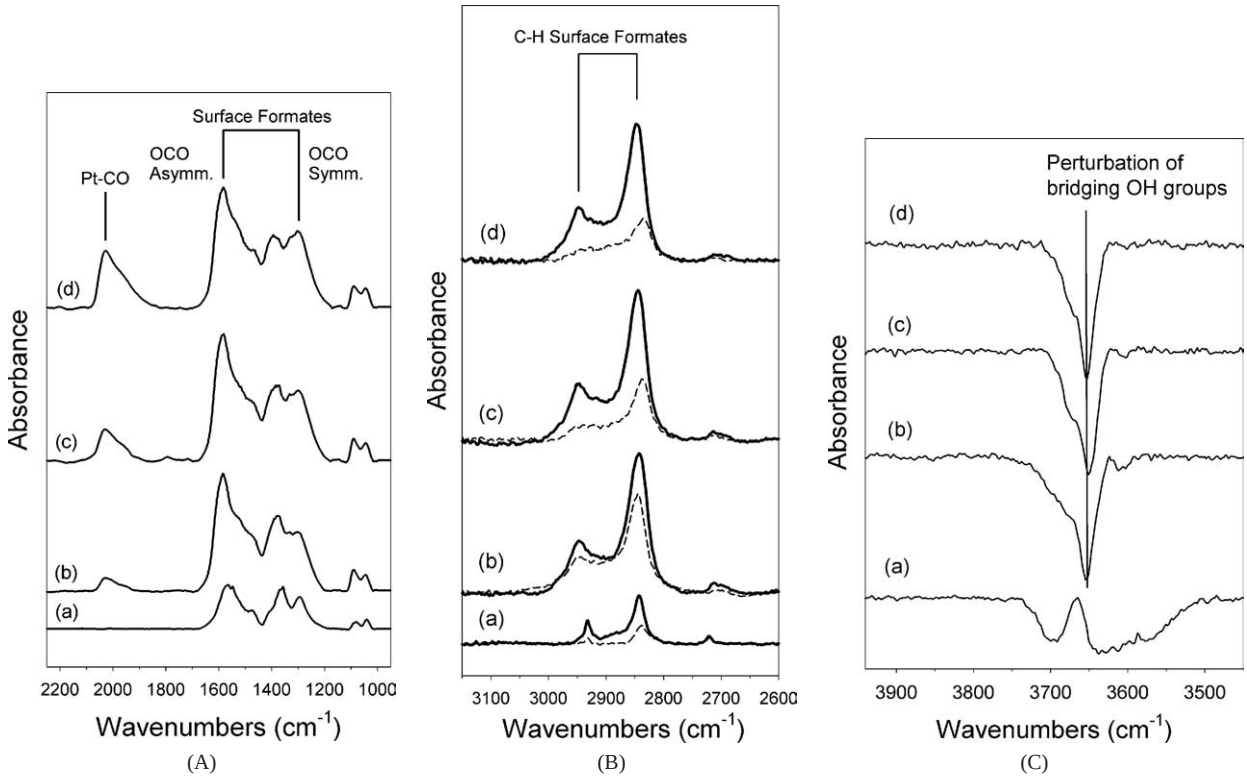

Fig. 8. (A) Adsorption of CO (33 mg catalyst, 3.75 cm^3/min CO, 135 cm^3/min N_2) to unpromoted and Pt/ceria catalysts reduced in H_2 at 250 °C, purged in N_2. OCO stretching region of surface formates. Moving upward, (a) unpromoted ceria, (b) 0.5%Pt/ceria, (c) 1.0%Pt/ceria, and (d) 2.5%Pt/ceria. (B) Adsorption of CO to unpromoted and Pt/ceria catalysts reduced in H_2 at 250 °C, purged in N_2 (33 mg catalyst). C–H stretching region of surface formates. Moving upward, (a) unpromoted ceria, (b) 0.5%Pt/ceria, (c) 1.0%Pt/ceria, and (d) 2.5%Pt/ceria. Note a systematic decrease in the formate coverage with increasing Pt loading under WGS (3.75 cm^3/min CO, 125 cm^3/min H_2O, 10 cm^3/min N_2). (C) Adsorption of CO to unpromoted and Pt/ceria catalysts reduced in H_2 at 250 °C, purged in N_2 (33 mg catalyst). Perturbation in the O–H stretching region accompanying CO adsorption (3.75 cm^3/min, 135 cm^3/min N_2). Moving upward, (a) unpromoted ceria, (b) 0.5%Pt/ceria, (c) 1.0%Pt/ceria, and (d) 2.5%Pt/ceria. Note the O–H groups on the Pt/ceria catalysts (b–d) are of the bridging (Type II) variety, which only occur on the surface of partially reduced ceria. (D) Due to the difference in background absorption, the 5%Pt/ceria (3.75 cm^3/min CO, 135 cm^3/min N_2) catalyst is reported separately. Changes during adsorption of CO in (a) the OH region; (b) the OCO region; and (c) the C–H stretching region. Dashed line in (c) shows the change after replacing nitrogen balancing gas with H_2O (3.75 cm^3/min CO, 125 cm^3/min H_2O, 10 cm^3/min N_2).

sorption bands in the OCO region (i.e., 1200–1650 cm^{-1} range) and the band intensities that remain after the surface reduction process at, for example, 250 °C provide a good indication of the extent to which the carbonate species have been removed, which allows for the generation of the bridging OH groups. Before surface reduction, bands for OH groups are observed in the range of 3690–3700 cm^{-1}. These are normally assigned to terminal OH groups on unreduced ceria surface (i.e., Type I OH groups [7–9]). However, accompanying partial reduction of ceria is the formation of Type II bridging OH groups on the partially reduced ceria surface, and a main band at 3650 cm^{-1}, with a shoulder at 3675 cm^{-1}, is observed [7,8,10].

Important differences are evident in the spectra for the hydrogen treatment (Fig. 7A) of unpromoted and Pt-promoted ceria catalysts with different amounts of Pt. For unpromoted ceria, a large amount of surface carbonate remains on the surface, even after reduction at 250 °C (Fig. 7A), as noted by the width of absorption bands in the OCO region between 1200 and 1650 cm^{-1}. Since the surface reduction process occurs for unpromoted ceria at temperatures greater than 400 °C, as indicated by TPR, the lowest intensity of bridging OH bands is obtained for the unpromoted catalyst at 250 °C (Fig. 7B, spectrum a). This is further supported by the low extent of ceria partial reduction by XANES analysis for the unpromoted sample after treatment at 250 °C in H_2.

The IR spectra for Pt/ceria catalysts are similar during the hydrogen reduction process. After hydrogen treatment at 250 °C, the width of absorption bands in the OCO region for residual surface carbonates was much narrower for the Pt-promoted catalysts in comparison with that of unpromoted ceria (Fig. 7A), and the Pt-promoted catalysts displayed much higher intensities of bridging OH groups after reduction at 250 °C (Fig. 7B). Again, these TPR and XANES results are in agreement with the Pt-catalyzed surface reduction process. Finally, although the single-beam spectra were especially attenuated for the 5.0% Pt/ceria catalyst, the changes were easily observed when the single-beam intensity spectra were multiplied by a factor of 3. It is apparent that the surface reduction process proceeds at even lower temperature with the 5.0% Pt/ceria catalyst (i.e., 150 °C), again supported by TPR and XANES results. This is evident

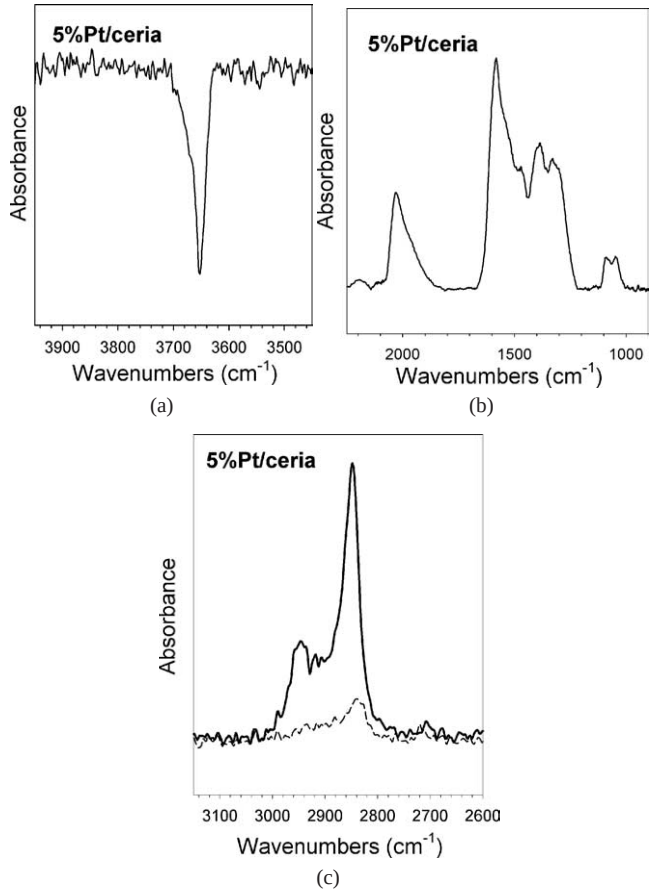

(D) DRIFTS results for 5% Pt/ceria

Fig. 8. Continued.

from the appearance of bands for the bridging OH groups at this temperature and, comparatively, the most significant loss of bands in the carbonate region (1200–1650 cm^{-1}) at 150 °C during H_2 treatment. Changes in the intensity and positions of carbonate bands have been observed during H_2 treatment in previous studies [7].

3.4.2. Adsorption of CO and water–gas shift

As CO is proposed to react with the bridging OH groups to generate the surface formate species, CO is an important probe molecule for the bridging OH group active site density. Those samples with a high density of bridging OH groups and, therefore, a higher extent of ceria partial reduction should exhibit a greater intensity of surface formate bands after CO adsorption. It is therefore anticipated that the unpromoted sample after low-temperature treatment in hydrogen, with its low density of bridging OH groups, should therefore yield a low intensity of surface formate species after the adsorption of CO. Figs. 8A–C show the changes that take place after CO is adsorbed at 250 °C to the H_2-treated samples of unpromoted and 0.5, 1.0, and 2.5% loaded Pt/ceria catalysts. In each case, for the Pt/ceria catalysts, bands consistent with the symmetrical (ca. 1300 cm^{-1}) and asymmetrical (ca. 1580 cm^{-1}) OCO vibrations (Fig. 8A) of surface formates are observed from the reaction of CO with the Type II bridging OH groups. Fig. 8B indicates that, accompanying these bands, are those of the C–H stretching vibrations (ca. 2845 and 2950 cm^{-1}). These may both be assigned to bidentate formate [21,22] or, possibly, to bidentate and a bridging-type formate, respectively, as has also been suggested [6]. With the production of these intense formate bands, the bridging OH groups decrease significantly, indicating that they are reacting with CO to produce the formates (Fig. 8C).

In a comparison of the unpromoted catalysts with the Pt/ceria catalysts (Figs. 8A–C), the intensities of OCO and C–H bands attributed to surface formates appear to be much lower for the unpromoted ceria than for the Pt/ceria catalysts. This again is in line with the previous comments regarding the surface reduction. The surface of ceria remains unreduced, such that the bridging OH group active sites are not formed; moreover, the surface carbonates are still abundant on the surface at 250 °C. Therefore, without formation of bridging OH groups, only very weak formate bands are produced upon adsorption of CO. From an examination of the Pt/ceria catalysts, even a small amount of Pt (e.g., 0.5%) can be seen to exert an important promotion on the surface reduction process. The decreases in the OH band intensities with CO adsorption occur at the same wavenumber position (ca. 3650 cm^{-1}) for the Pt-promoted catalysts (Fig. 8C), whereas the changes in the OH region of the unpromoted catalyst were very weak and apparently were associated with Type I OH groups situated at ca. 3700 cm^{-1} (Fig. 8C, spectrum a). It is important to note that the changes in background absorption observed in the change to more heavily loaded Pt catalysts make precise quantification of the surface formate concentrations between samples difficult; therefore, we limit the discussion to the relative changes occurring for each specific sample.

In WGS conditions, 125 of the 135 cm^3/min N_2 was replaced with H_2O in order to (a) maintain a constant CO partial pressure, (b) maintain a constant space velocity, and (c) provide a high H_2O/CO ratio, so that the reaction order of H_2O partial pressure is close to zero, and that of CO is close to unity. These are conditions whereby the active surface should be close to saturation during WGS by an adsorbed H_2O species, whereas the adsorbed CO intermediate should be responsive to the WGS rate. That is, the experiments were not conducted under conditions where the adsorbed CO intermediate is expected to be at saturation during WGS (e.g., a high CO/H_2O ratio). It is important to note that in a fuel processor for fuel cell applications, very low CO/H_2O ratios are typical. There is an important decrease in the C–H stretching band of surface formates for each of the Pt/ceria catalysts (Fig. 8B, dotted line spectra). There is also a systematic decrease in the surface formate band intensity under WGS conditions with increasing Pt loading. This indicates that, with higher Pt loading, the WGS rate may be higher partly because of the faster decomposition of surface formates. Although the sample exhibited a much weaker signal

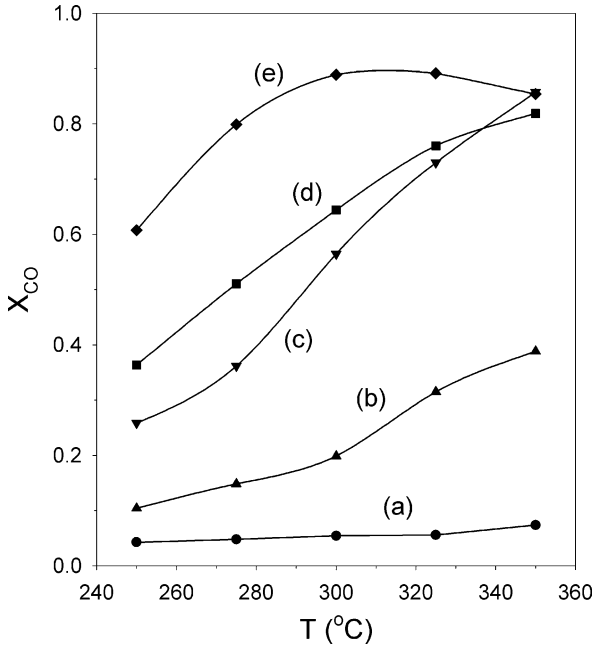

Fig. 9. CO conversion as a function of temperature for different Pt loadings (3.75 cm^3/min CO, 125 cm^3/min H_2O, 100 cm^3/min H_2, 10 cm^3/min N_2) for, moving upward, (a) unpromoted ceria; (b) 0.5%Pt/ceria; (c) 1.0%Pt/ceria; (d) 2.5%Pt/ceria; and (e) 5.0%Pt/ceria. Data obtained from fixed bed reactor testing (33 mg catalyst).

due to background absorption, the greatest change in formate coverage in the switch from CO adsorption to WGS conditions was observed for the 5% Pt/ceria catalyst (Fig. 8D, spectrum c). Although total site densities are expected to vary with the partial reduction of ceria, the formate coverages are provided in Table 3. Note that, under all conditions, the Pt–CO coverage decreased only slightly, indicating that adsorbed CO on Pt is likely not the important adsorbed CO intermediate for the low-temperature shift mechanism.

3.5. *Catalytic activity tests*

Consistent with the in situ DRIFTS experiments, the more heavily loaded Pt catalysts displayed higher CO conversion during WGS over the temperature range from 250 to 350 °C, as shown in Fig. 9. As the bridging OH groups were not activated, in the case of the unpromoted catalyst (activation temperature of 450 °C required by TPR experiments), the catalyst displayed very low activity over the entire temperature range.

The increased CO conversion rate with Pt loading is consistent with the findings from the ceria partial reduction experiments obtained by XANES and TPR and the formate coverage dynamics investigation by DRIFTS. At higher Pt loading, enhanced partial reduction of ceria at low temperatures is consistent with higher active site densities of bridging OH groups associated with the Ce^{3+} defect centers. At higher Pt loading, the formate decomposition rate is suggested by in situ DRIFTS findings to be accelerated. Therefore, Pt may participate in the reaction mechanism to enhance the surface formate decomposition, indicating a possible benefit in catalytic activity on a per active site basis.

4. Discussion

This study underscores the important link between CO conversion and the number of reduced Ce^{3+} centers in the surface shell. The generation of these reduced centers is facilitated by the presence of the Pt promoter, and increased Pt loading was found to directly affect catalytic activity.

The ability of the metal to promote reduction of ceria is not a new concept. In fact, such findings have recently led to the proposal of the widely recognized ceria-mediated redox mechanism [12,23–25]:

$$Pt^* + CO \rightarrow Pt\text{–}CO,$$

$$Pt\text{–}CO + 2CeO_2 \rightarrow Ce_2O_3 + CO_2 + Pt^*,$$

$$Ce_2O_3 + H_2O \rightarrow 2CeO_2 + H_2.$$

In a consideration of the redox mechanism, where reaction of H_2O with reduced Ce^{3+} centers is suggested to release hydrogen, an increase in the number of reduced centers (in this case vacancies) would be anticipated to lead to improved active site densities. Therefore, we do not rule out the possibility of a redox mechanism.

However, there are a number of reasons why we consider a formate mechanism to be more plausible under the high H_2O/CO feed ratio found in a fuel cell processor for purification of hydrogen. In considering the active site bridging OH groups, it is important to first realize that they also occur at reduced Ce^{3+} defect centers. The proposed mechanism of Shido and Iwasawa [5,6] provides a viewpoint whereby water dissociates over vacancies of ceria (in that case, promoted with Rh) to generate the bridging OH groups, as shown in Scheme 2. This highlights the importance of reduced Ce^{3+} centers for that proposed mechanism. Therefore, promoting the reduction of ceria with increasing Pt loading would be expected to lead to higher active site densities of bridging OH groups. We also point out in Scheme 2 that once a noble metal promoter, like Pt, is reduced, H_2 can dissociate and spill over to the surface of ceria, thereby generating the bridging OH groups directly, a process that must also be accompanied by a change in the oxidation state of the Ce atoms involved with the OH groups from Ce^{4+} to Ce^{3+}.

The results of TPR and XANES clearly indicate that increasing the Pt loading facilitates the Ce surface reduction process. However, the XANES data for the Pt L_{III} edge show that for the lowest loadings of Pt, the reduction of the Pt oxide clusters is hindered, whereas the more heavily loaded Pt/ceria catalysts offer much more facile reduction at temperatures as low as 100 °C, as observed for the 5% Pt/ceria catalyst. This result is consistent with our consideration that the Type II bridging OH groups can be formed directly from H_2 dissociation over Pt^0 and spillover to the ceria surface, such that the Ce^{4+} atoms involved with the bridging OH

Table 3
Relative formate and Pt–CO intensities at 250 °C

I	Pt (%)	$I_{\text{formate, CO}}$ (absorb.)	$I_{\text{formate, WGS}}$ (absorb.)	$\theta_{\text{formate, WGS}}$	$I_{\text{Pt–CO, CO}}$ (absorb.)	$I_{\text{Pt–CO,WGS}}$ (absorb.)	$\theta_{\text{Pt–CO, WGS}}$
1	0.5	0.213	0.162	0.7596	0.079	0.073	0.9241
2	1	0.227	0.085	0.3744	0.134	0.124	0.9254
3	2.5	0.214	0.059	0.2754	0.318	0.289	0.9088
4	5.0[a]	0.0921	0.0120	0.1303	0.180	0.178	0.9888

[a] Note that the background absorption for this sample was much higher than the others.

group formation change oxidation state to Ce^{3+}. The Pt clusters at heavier loadings would likely be larger on average, rendering them able to overcome the metal–oxide interaction at lower temperatures.

In Fischer–Tropsch synthesis, a reduction promoter metal is often used to aid in catalyzing the reduction of cobalt oxide species strongly interacting with a γ-Al_2O_3 support. In that way, the aim was to improve the percentage reduction of cobalt and generate additional cobalt metal clusters to increase catalyst activity on a per-gram basis. Optimization of the promoter loading was necessary, as systematic shifts to lower temperatures of the cobalt oxide reduction were observed with increasing noble metal promoter loading until a loading limit was reached, whereby further promotion was not observed [26]. That process involved overcoming the support interaction with the metal. In the present case, a similar effect is observed with increased Pt promoter loading. That is, a systematic decrease in the temperature required for the surface reduction of ceria is observed. At 5% Pt loading, the ceria surface shell reduction temperature has shifted from ca. 450 °C (in the case of the unpromoted catalyst) to 150 °C for the highest Pt loading. Those who support a ceria-mediated redox process would suggest that the redox pair can therefore take place at the lower temperature. Those who favor a surface formate mechanism to explain the WGS mechanism would argue that the bridging OH groups (i.e., active sites) are able to form at the lower temperature.

The correct mechanism is not obvious, highlighting the important need to invoke kinetic arguments and utilize techniques to probe the mechanism, such as the identification of a possible kinetic isotope effect and steady-state isotopic transient kinetic analysis combined with in situ infrared spectroscopy [27].

In fixed-bed catalytic testing, we have observed a normal kinetic isotope effect (KIE), in agreement with Shido and Iwasawa [6], and by two in situ infrared experiments aimed at examining the response of surface formates (steady state [28] and transient [10]), the normal KIE was suggested to be linked to the breaking of the formate C–H bond. It is of interest to note that the kinetic isotope effect was virtually identical to that observed in the decomposition of formic acid, where we switched between HCOOH and DCOOH feeds [submitted]. FTIR results indicated the H- and D-formates generated in that study via dissociative adsorption of formic acid were identical to those produced from the reaction of CO with the bridging OH groups in our WGS investigations, results which are in line with the interpretation of the heterogeneous catalytic mechanism proposed by Mars et al. (and references therein) about 50 years ago [29].

Our most recent results in support of a formate mechanism for low-temperature WGS come from steady-state isotope switching transient kinetic analysis, where the exchange rates of ^{12}CO to ^{13}CO for surface species were measured by in situ DRIFTS under real WGS conditions [Catal. Lett., in press]. Briefly, at 225 °C in the absence of H_2O (and therefore, no WGS reaction), formates were observed to be quite stable on the surface, whereas Pt–CO rapidly exchanged from ^{12}CO to ^{13}CO. However, when the inert balancing gas was replaced by H_2O, formates also rapidly exchanged to produce $H\,^{13}CO_2^-$, and the CO_2 product exchange was in parallel with that of the formate exhange.

From a kinetic point of view, the WGS rate over metal/ceria catalysts has been found to follow a standard Langmuir–Hinshelwood-type expression [12] of the form

$$r = k_1 k_2 P_{CO} P_{H_2O} / (k_1 P_{CO} + k_2 P_{H_2O}).$$

If we consider a high CO/H_2O partial pressure ratio, the rate is zero order in P_{CO} and first order in P_{H_2O}, such that the adsorbed CO intermediate should be close to saturation during WGS. The opposite should be true under fuel processor conditions for low-temperature shift, where high H_2O/CO ratios are typical. The reaction order for P_{H_2O} should be zero, whereas P_{CO} should be close to first order. Under WGS conditions, the adsorbed H_2O surface species should therefore be close to saturation, and certainly the amount of bridging OH groups fits that criterion. The adsorbed CO intermediate coverage, however, should be controlled by the WGS rate; that is, the faster the WGS rate, the lower the concentration of surface formates.

We have previously conducted in situ DRIFTS investigations [30,31] in a flow mode where a $CO:N_2$ mixture was first introduced to establish a surface concentration of adsorbed CO species. Then, maintaining a constant P_{CO}, we switched from a feed containing 3.75 cm^{-3} CO:135 cm^{-3} N_2 to a WGS feed containing 3.75 cm^{-3} CO:125 cm^{-3} H_2O:10 cm^{-3} N_2. This switch was carried out at different temperatures. Whereas Pt–CO did not change appreciably in coverage, surface formates were found to be controlled by the WGS rate. Transient switching experiments were also carried out [18], whereby formates were loaded onto the surface by reaction of CO with the bridging OH groups,

followed by reaction of the formates with H_2O. CO_2 was clearly generated by the formate decomposition.

This procedure was similarly carried out over the series of Pt/ceria catalysts with increasing Pt loading, but at the same temperature. For the catalysts with higher Pt loading, the formate coverages were more reaction rate limited on the surface when we switched to the WGS feed. Again, Pt–CO coverage did not reveal an important change.

From this study, it appears that Pt may be directly involved in the mechanism, but not in the same way as indicated by the ceria-mediated redox process [12,23–25], where it is reaction of Pt–CO with CeO_2 at the interface that generates CO_2 and a vacancy. Rather, from the in situ DRIFTS data, it is suggested that Pt may accelerate the decomposition rate of the surface formates. However, it is not clear at this time how this is accomplished.

5. Conclusions

Increasing the Pt loading had a significant impact on the catalytic activity. The partial reduction of ceria is necessary for generating bridging OH groups on the surface of ceria, which serve as the active sites. During this surface shell reduction process in hydrogen, surface carbonates are liberated, hydrogen is dissociated to produce two bridging OH groups, and two cerium atoms for each dissociated hydrogen molecule change from the Ce^{4+} to the Ce^{3+} oxidation state. Addition of Pt catalyzes the surface reduction process and reduces the peak reduction temperature from 450 °C for the unpromoted catalyst to 150 °C for the 5% Pt/ceria catalyst. Whereas addition of CO to the unpromoted catalyst reduced at 250 °C led to only very weak formate bands due to the limited number of bridging OH groups at that temperature, strong formate bands arose on the surface of the Pt/ceria catalysts at 250 °C. In situ DRIFTS was used to probe the dynamics of the surface formate coverages, and links were established between the response of the formate coverages under WGS and the resulting catalytic activity. Of particular interest is the observation that the surface formates on the more highly loaded Pt/ceria catalysts were the most reaction rate limited under WGS after we switched from CO adsorption alone to the WGS condition. The results indicate not only that Pt serves to facilitate the generation of the bridging OH groups (active sites) at low temperature, but that it may also be involved in accelerating the decomposition of surface formates, the proposed rate-limiting step of the reaction mechanism. HR-TEM indicates that both Pt clusters and ceria domains are on the order of nanometers, emphasizing the importance of catalyst design at the nanoscale.

Acknowledgments

This work was supported by the Commonwealth of Kentucky. We especially thank Dr. Syed Khalid for all of his help in setting up experiments at Beamline X-18b at the National Synchrotron Light Source located at Brookhaven National Laboratory in Upton, New York, and Joel Young at the University of Oklahoma's Department of Physics for fabrication of the in situ X-ray spectroscopy cell. Research carried out (in part) at the NSLS, at BNL, is supported by the US Department of Energy, Division of Materials Science and Division of Chemical Sciences, under contract no. DE-AC02-98CH10886.

References

[1] National Hydrogen Energy Roadmap, US DOE (2002).
[2] Fuel Cell Report to Congress, US DOE (2003).
[3] D.C. Dayton, M. Ratcliff, R. Bain, Fuel Cell Integration—A Study of the Impact of Gas Quality and Impurities, NREL/MP-510-30298 (2001).
[4] A.F. Ghenciu, Curr. Opin. Solid State Mat. Sci. 6 (2002) 389.
[5] T. Shido, Y. Iwasawa, J. Catal. 141 (1993) 71.
[6] T. Shido, Y. Iwasawa, J. Catal. 136 (1992) 493.
[7] A. Laachir, V. Perrichon, A. Badri, J. Lamotte, E. Catherine, J.C. Lavalley, J. El Fallah, L. Hilaire, F. Le Normand, E. Quemere, G.N. Sauvion, O. Touret, J. Chem. Soc., Faraday Trans. 87 (1991) 1601.
[8] J. Lamotte, J.C. Lavalley, E. Druet, E. Freund, J. Chem. Soc., Faraday Trans. 79 (1983) 2219.
[9] A. Holmgren, B. Andersson, D. Duprez, Appl. Catal. B 22 (1999) 215.
[10] G. Jacobs, P. Patterson, L. Williams, U. Graham, D.E. Sparks, B.H. Davis, Appl. Catal. A: Gen. 269 (2004) 63.
[11] G. Jacobs, E. Chenu, P. Patterson, L. Williams, D. Sparks, B.H. Davis, Appl. Catal. 258 (2004) 203.
[12] Y. Li, Q. Fu, M. Flytzani-Stephanopoulos, Appl. Catal. B 27 (2000) 179.
[13] T. Ressler, WinXAS 97 version 1.0 (1997).
[14] G. Jacobs, P. Patterson, L. Williams, E. Chenu, D. Sparks, G. Thomas, B.H. Davis, Appl. Catal. A 262 (2004) 177.
[15] H.C. Yao, Y.F.Y. Yao, J. Catal. 86 (1984) 254.
[16] K.T. Jung, A.T. Bell, Catal. Lett. 80 (2002) 63.
[17] G. Jacobs, A. Crawford, L. Williams, P.M. Patterson, B.H. Davis, Appl. Catal. A: Gen. 267 (2004) 27.
[18] G. Jacobs, P.M. Patterson, L. Williams, D.E. Sparks, B.H. Davis, Catal. Lett. 96 (2004) 97.
[19] S. Overbury, D. Huntley, D. Mullins, G. Glavee, Catal. Lett. 51 (1998) 133.
[20] J. El Fallah, S. Boujani, H. Dexpert, A. Kiennemann, J. Majerus, O. Touret, F. Villain, F. Le Normand, J. Phys. Chem. 98 (1994) 5522.
[21] C. Li, Y. Sakata, T. Arai, K. Domen, K. Maruya, T. Onishi, J. Chem. Soc., Faraday Trans. 1 85 (1989) 1451.
[22] C. Li, K. Domen, K.-I. Maruya, T. Onishi, J. Catal. 125 (1990) 445.
[23] S. Hilaire, X. Wang, T. Luo, R.J. Gorte, J. Wagner, Appl. Catal. 215 (2001) 271.
[24] T. Bunluesin, R. Gorte, G. Graham, Appl. Catal. B 15 (1998) 107.
[25] Q. Fu, A. Weber, M. Flytzani-Stephanopoulos, Catal. Lett. 77 (1–3) (2001) 87.
[26] G. Jacobs, T.K. Das, Y. Zhang, J. Li, G. Racoillet, B.H. Davis, Appl. Catal. A: Gen. 233 (2002) 263.
[27] D. Tibiletti, A. Goguet, F.C. Meunier, J.P. Breen, R. Burch, Chem. Commun. 14 (2004) 1636.
[28] G. Jacobs, S. Khalid, P.M. Patterson, L. Williams, D.E. Sparks, B.H. Davis, Appl. Catal. 268 (2004) 255.
[29] P. Mars, J.J.F. Scholten, P. Zwietering, Adv. Catal. 14 (1963) 35.
[30] G. Jacobs, L. Williams, U. Graham, D.E. Sparks, B.H. Davis, J. Phys. Chem. B 107 (2003) 10398.
[31] G. Jacobs, L. Williams, U. Graham, D.E. Sparks, G. Thomas, B.H. Davis, Appl. Catal. A 252 (2003) 107.